TWO-PHASE CONTINUUM MODELLING OF COMPOSITES CONSOLIDATION

Maciej Wysocki[1*], Leif E. Asp[1], Staffan Toll[2] and Ragnar Larsson[2]

[1]Swerea SICOMP AB, Box 104, 431 22 Mölndal, Sweden
[2]Chalmers Unicersity of Technology, 412 96 Göteborg, Sweden
[*]maciej.wysocki@swerea.se

ABSTRACT

In this paper a finite element code for modelling of pressure driven axisymmetric consolidation of composite material from commingled yarns is presented. The proposed model is developed on the basis of a two-phase continuum model incorporated in a FE-framework. The applicability of the code to axisymmetric geometries is demonstrated by analysis of the consolidation, i.e. resin infiltration and fibre bundle network deformation, of a GF/PP pressure vessel. In this numerical example two different sets of processing conditions are presented. Based on these analysis results conclusions on the process ability of the investigated vessel configuration and manufacturing scheme are drawn and processing recommendations are given.

1. INTRODUCTION

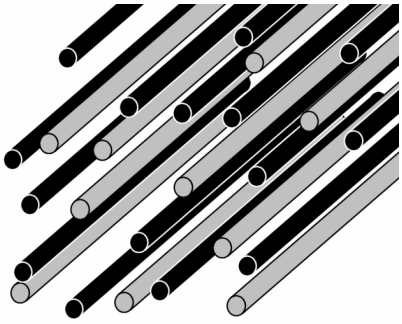

Figure 1. Pre-impregnation by commingling of thermoplastic and reinforcing fibres.

Thermoplastic matrix composites are considered the composites of the future. However, their use has been hampered by the difficulty with which they are manufactured. That is, thermoplastic polymers exhibit significantly higher viscosity than do thermoset resins – this may be illustrated comparing the difference in the flow properties between chewing gum and olive oil. Composite manufacture involves wetting of very large fibre area. Consequently, the difficulty experienced in manufacture of thermoplastic matrix composites is related to the polymer flow and impregnation of the reinforcing fibres. Manufacturing processes to mitigate this problem have been developed [1], processing the composite in two steps: pre-impregnation and moulding. The pre-impregnation yields a semi-product, in which the thermoplastic has been dispersed in the fibre network, minimising the distance the polymer must flow to wet the fibres, yet no wetting has taken place to keep the semi-product flexible. Commingling of thermoplastic fibres with the reinforcing fibres is one

of the most promising routes for pre-impregnation, see Figure 1, featuring relatively high and uniform pre-impregnation quality at low cost.

The composite structure is manufactured by a moulding operation where a chosen pre-impregnated system lay-up is heated and pressed into its final shape. During this moulding operation three different tasks are performed: wetting of the fibres by the molten polymer, forming into shape and, in some cases, macroscopic drainage of resin. In the most efficient processes all these tasks are performed simultaneously. Today, the materials and manufacturing technology are available, however, the capability to model the manufacturing process is limited. A comprehensive description of the state-of-the-art in process simulation of thermoplastic composite materials is given in a recent paper by Wysocki et al. [2].

Recently, a continuum thermodynamic framework for the purpose of thermoplastic matrix composites process simulation [3], [2] has been developed. In [3], a two-phase continuum model incorporating the important phenomenon of fibre bundle elasticity and wetting was formulated. In the second paper [2], the framework was expanded as the constitutive equations governing the hydrostatic consolidation of commingled yarn based composites were established and introduced into the continuum mechanical framework.

The objective of the present study is to formulate and demonstrate a finite element model for axisymmetric consolidation of commingled yarn – based composites. The outline of the paper is as follows: the theoretical models and their computational implementation are briefly described. The following formulation of the axisymmetric boundary condition and its implementation in the framework is described in detail. Computational results from a numerical example (pressure vessel) are then presented and discussed. Finally, the results are discussed and conclusions are drawn.

2. THEORETICAL AND NUMERICAL MODEL

In the following section an overview of the theoretical foundation for modelling of the deformation and consolidation and the resulting numerical methods are presented. Detailed theoretical descriptions of the model are given in references [2] and [3].

2.1 Constituents and deformation processes

The approach taken is to model composite consolidation adopting a two-phase continuum consideration of the three constituents, fibres, matrix and voids; where the treatment of fibres and voids is simplified by associating them with one continuum phase, the solid phase. The matrix is represented by the second continuum phase, the liquid.

The solid and fluid phases are denoted *s* and *f*, respectively. Their volume fractions n^s and n^f are defined in terms of the constituents as:

$$n^s(\mathbf{x},t) = \phi^p(\mathbf{x},t) + \phi^v(\mathbf{x},t) \text{ and } n^f(\mathbf{x},t) = \phi^l(\mathbf{x},t), \tag{1}$$

where ϕ^p is the particle volume fraction, ϕ^v the void volume fraction and ϕ^l the liquid volume fraction. The intrinsic density, associated with each phase, is denoted ρ^α, where $\alpha = s,\ f$, whereby, using the indicator function χ^α, the bulk density per unit bulk volume is obtained as

$$\hat{\rho}^\alpha(\mathbf{x},t) = \frac{1}{v}\int_v \rho^\alpha(\mathbf{x},t)\,\chi^\alpha(\mathbf{x},t)\,d\mathbf{x} = n^\alpha(\mathbf{x},t)\,\rho^\alpha(\mathbf{x},t) \text{ with } \alpha = s,\ f\,. \tag{2}$$

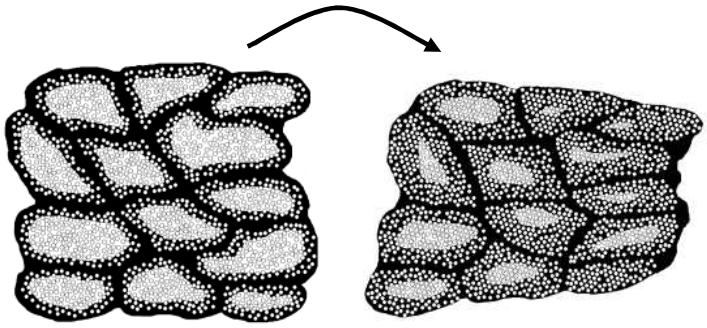

Figure 2. Schematic of the assumed inter-bundle processes consisting of elastic deformation and matrix flow between the bundles.

During press forming of this multi-constituent material system, four primary modes of deformation can be identified. These are the two processes at the meso-scale due to inter-bundle deformation and the two processes at the micro-scale due to intra-bundle deformation. It is assumed that the meso-scale processes, conceptually depicted in Figure 2, are governed by elastic interaction and matrix flow, i.e. macroscopic drainage, between the bundles. Furthermore, it is noticed that these processes are controlled by the macroscopic tractions and deformations. The micro-scale processes, on the other hand, are assumed to be governed by the elastic interaction within the bundles and the process of matrix infiltration into the bundles, cf. Figure 2.

2.2 A two-phase continuum model

Following the development in [4], it is assumed that each spatial point of the mixture is simultaneously occupied by particles from the solid and fluid phase. Upon deformation the continuum phases move via individual non-linear deformation maps, φ^s and φ^f, defined as

$$\mathbf{x} = \boldsymbol{\varphi}^{\alpha}\left(\mathbf{X}^{\alpha}, t\right),\ \alpha = s, f\ , \tag{3}$$

where $\mathbf{x}$ denotes the current position of a continuum particle $\mathbf{X}^{\alpha}$ at the time t.

From equilibrium considerations [3], the continuum momentum balance for the mixture is obtained as

$$\operatorname{div}\overline{\boldsymbol{\sigma}} + \hat{\rho}\mathbf{g} = \mathbf{0}\,, \tag{4}$$

where $\overline{\boldsymbol{\sigma}} = \boldsymbol{\sigma}^s + \boldsymbol{\sigma}^f$ is the total Cauchy stress and $\hat{\rho} = \hat{\rho}^s + \hat{\rho}^f$ is the density of the mixture.

Due to mass conservation during deformation of the two-phase continuum [3], the balance of mass for the mixture may be formulated as

$$\operatorname{div}\mathbf{v} - n^s\dot{\varepsilon} = -\operatorname{div}\mathbf{v}^d \tag{5}$$

where $\mathbf{v}$ is the solid phase velocity, $\mathbf{v}^d := n^s\left(\mathbf{v}^f - \mathbf{v}^s\right)$ is the Darcian velocity and ε is the logarithmic volumetric strain in the solid phase defined as

$$\varepsilon = -\ln\frac{\rho^s}{\rho_0^s}\,. \tag{6}$$

The local form of the internal energy balance for the mixture per unit mass [3] may be written as

$$\dot{\bar{e}} = \overline{\boldsymbol{\sigma}} : \mathbf{l} - p\operatorname{div}\mathbf{v}^d + \mathbf{v}^d \cdot \left(\rho^f\mathbf{g} - \rho^f\nabla e^f - \nabla p\right), \tag{7}$$

where e^f represents the internal energy for the fluid phase, $\mathbf{l} = \mathbf{v} \otimes \nabla_{\mathbf{x}} = \dot{\mathbf{F}} \cdot \mathbf{F}^{-1}$ is the spatial velocity gradient and $\mathbf{F} = \boldsymbol{\varphi} \otimes \nabla_{\mathbf{x}}$ is the deformation gradient. The localised form of the entropy inequality for the mixture is now specified as

$$\mathcal{D} = \dot{\bar{s}} + \rho^f \mathbf{v}^d \cdot \nabla s^f \geq 0 . \tag{8}$$

Moreover, by introducing entropy production in terms of internal energy and Helmholtz free energy, ψ, the equation (8) transforms to

$$\mathcal{D} = \dot{\bar{e}} - \dot{\bar{\psi}} + \rho^f \mathbf{v}^d \cdot \nabla s^f \geq 0 . \tag{9}$$

Finally, upon combining (9) with (7) and (6) the entropy inequality for the solid-fluid interaction is obtained as

$$\mathcal{D} = \boldsymbol{\sigma} : \mathbf{l} - n^s p \dot{\varepsilon} - \hat{\rho}^s \dot{\psi} - \mathbf{h}_e^f \cdot \mathbf{v}^d \geq 0 , \tag{10}$$

where $\boldsymbol{\sigma} = \bar{\boldsymbol{\sigma}} + p\mathbf{1}$ is the Terzaghi effective stress and $\mathbf{h}_e^f$ is the effective drag force defined as $\mathbf{h}_e^f = \nabla p - \rho^f \mathbf{g}$.

2.3 Constitutive models

For simplicity, it is assumed that there is no coupling on the constitutive level between the fibre network deformation in terms of the right Cauchy-Green deformation tensor, **C**, and the intrinsic compaction, ε. Moreover, the intrinsic compaction due to matrix infiltration is represented as an internal variable denoted, ε^p, and the free energy is assumed to possess the additive structure

$$\psi = \psi\left(\mathbf{C}, \varepsilon, \varepsilon^p\right) = \psi^1\left(\mathbf{C}\right) + \psi^2\left(\varepsilon, \varepsilon^p\right). \tag{11}$$

The constitutive equations are established by distinguishing three different types of dissipative mechanism of the total dissipation defined as

$$\mathcal{D} = \underbrace{\boldsymbol{\sigma} : \mathbf{l} - \hat{\rho}^s \dot{\psi}^1}_{\mathcal{D}_1} \underbrace{- n^s p \dot{\varepsilon} - n^s \rho^s \dot{\psi}^2}_{\mathcal{D}_2} \underbrace{- \boldsymbol{h}_e^f \cdot \boldsymbol{v}^d}_{\mathcal{D}_3} \geq 0 , \tag{12}$$

where the dissipative mechanism $\mathcal{D}_1$, is due to effective stress response, $\mathcal{D}_2$ is due to fluid pressure, and $\mathcal{D}_3$ due to macroscopic Darcy flow. Note, that these mechanisms correspond to the material responses of (i) elastic interaction between bundles, (ii) wetting and compressing of fibre bundles by the liquid resin and (iii) matrix flow between bundles, i.e. macroscopic drainage. Full theoretical descriptions of $\mathcal{D}_1$ and $\mathcal{D}_2$ are given in references [3] and [2], respectively, whereas a theoretical model for $\mathcal{D}_3$ is found in the paper by Larsson and Larsson [4].

3. BOUNDARY VALUE PROBLEM

In this section the formulation of the boundary value problem and the corresponding finite element formulation for modelling the axisymmetric consolidation are described. The model is developed considering composite manufacturing using a press forming process. In the studied process, the component (in this case a pressure vessel) is subjected to an external uniform pressure sufficient to drive the infiltration of resin into the bundles. However, the overall pressure gradients are too weak to drive any significant macroscopic Darcy flow, therefore it is assumed that $\mathcal{D}_3 \equiv 0$. Thus, the subsequent development is specialised to the undrained condition.

3.1 Weak formulation of momentum balance

In order to formulate the finite element solution, the weak form of the momentum balance for the mixture of solid and fluid phases is written in terms of the balance between internal virtual work G^{int} and external virtual work G^{ext}

$$G^{\text{int}} - G^{ext} = 0\,, \tag{13}$$

where, omitting the volume loadings, the following expressions are derived

$$\begin{aligned} G^{\text{int}} &= \int_{B_0} \delta\mathbf{l} : \bar{\boldsymbol{\tau}}\, dV, \\ G^{ext} &= \int_{\partial B} \delta\boldsymbol{\varphi} \cdot \mathbf{t}\, ds, \end{aligned} \tag{14}$$

here $\bar{\boldsymbol{\tau}}$ is the total Kirchhoff stress and $\mathbf{t}$ is the prescribed nominal traction vector at the external boundary defined in terms of applied pressure, p^{ext}, as $\mathbf{t} = p^{ext}\,\mathbf{n}$. Consequently, pull-back to the reference configuration and definition of total Kirchhoff stress gives

$$\begin{aligned} G^{\text{int}} &= \int_{B_0} \delta\mathbf{l} : \left(\boldsymbol{\tau} - J\, p\mathbf{1}\right) dV, \\ G^{ext} &= \int_{\partial B_0} -p^{ext}\delta\boldsymbol{\varphi} \cdot J\,\mathbf{F}^{-t} \cdot \mathbf{N}\, dS. \end{aligned} \tag{15}$$

The linearised weak form of the internal virtual work of the mixture was derived by Larsson et al. [3] and is expressed for an incompressible fluid as

$$\dot{G}^{\text{int}} = \int_{B_0} \delta\mathbf{l} : \left(\mathbf{E}_2 + \mathbf{1} \bar{\otimes} \bar{\boldsymbol{\tau}} - J\, p\left(\mathbf{1}\otimes\mathbf{1} - 2\mathbf{I}^{sym}\right) + K^s \frac{J}{J - \left(1 - n_0^s\right)} \mathbf{1}\otimes\mathbf{1} \right) : \mathbf{l}\, dV\,. \tag{16}$$

The linearised weak form of the external virtual work of the mixture is obtained via linearisation of the term $J\mathbf{F}^{-t}\cdot\mathbf{N}$ in (16):

$$\frac{D}{Dt}\left(J\mathbf{F}^{-t}\cdot\mathbf{N}\right) = \mathbf{F}^{-t}\cdot\mathbf{N}\,\dot{J} + J\,\dot{\mathbf{F}}^{-t}\cdot\mathbf{N}\,, \tag{17}$$

which, by using relations $\dot{J} = J\,\mathbf{F}^{-t} : \dot{\mathbf{F}} = J\,\mathbf{1} : \mathbf{l}$ and $\dot{\mathbf{F}}^{-t} = -\mathbf{F}^{-t}\cdot\dot{\mathbf{F}}^{t}\cdot\mathbf{F}^{-t}$, becomes

$$\mathbf{F}^{-t}\cdot\mathbf{N}\, J\,\mathbf{F}^{-t} : \dot{\mathbf{F}} - J\,\mathbf{F}^{-t}\cdot\dot{\mathbf{F}}^{t}\cdot\mathbf{F}^{-t}\cdot\mathbf{N} = \left(J\mathbf{F}^{-t}\cdot\mathbf{N}\otimes\mathbf{F}^{-t} - \left(\mathbf{F}^{-t} \underline{\otimes} \left(\mathbf{F}^{-t}\cdot\mathbf{N}\right)\right)\right) : \dot{\mathbf{F}}\,. \tag{18}$$

The linearised weak form of the external virtual work of the mixture is finally obtained as

$$\dot{G}^{ext} = \int_{\partial B_0} p^{ext}\delta\boldsymbol{\varphi}\cdot\left(J\mathbf{F}^{-t}\cdot\mathbf{N}\otimes\mathbf{1} - \left(\mathbf{F}^{-t} \underline{\otimes} \left(\mathbf{F}^{-t}\cdot\mathbf{N}\right)\right)\cdot\mathbf{F}^{t}\right) : \mathbf{l}\, dS\,. \tag{19}$$

3.2 Finite element implementation for the axisymmetric problem

In the special case of axisymmetry, the momentum balance for the mixture of solid and fluid phases reads

$$2\pi\int_{\Omega_0} \delta\mathbf{l} : \left(\boldsymbol{\tau} - J\, p\mathbf{1}\right) R\, d\Omega - 2\pi\int_{\partial\Omega_0} -p^{ext}\delta\boldsymbol{\varphi}\cdot J\,\mathbf{F}^{-t}\cdot\mathbf{N} R\, dL = 0\,, \tag{20}$$

where Ω is a section through the axisymmetric body and R is the distance from the symmetry axis. Equivalently, the linearised internal and external virtual work of the mixture is obtained as

$$\dot{G}^{\text{int}} = 2\pi \int_{\Omega_0} \delta\mathbf{l} : \left(\mathbf{E}_2 + \mathbf{1} \bar{\otimes} \bar{\boldsymbol{\tau}} - J\, p\left(\mathbf{1}\otimes\mathbf{1} - 2\mathbf{I}^{sym}\right) + K^s \frac{J}{J - \left(1 - n_0^s\right)} \mathbf{1}\otimes\mathbf{1} \right) : \mathbf{l}\, R d\Omega,$$
$$\dot{G}^{ext} = 2\pi \int_{\partial\Omega_0} p^{ext} \delta\boldsymbol{\varphi} \cdot \left(J\mathbf{F}^{-t} \cdot \mathbf{N} \otimes \mathbf{1} - \left(\mathbf{F}^{-t} \underline{\otimes} \left(\mathbf{F}^{-t} \cdot \mathbf{N} \right) \right) \cdot \mathbf{F}^t \right) : \mathbf{l}\, R dL. \tag{21}$$

In equations (20) and (21) the deformation gradient is specialised to the axisymmetric case as

$$\mathbf{F} = \begin{pmatrix} \varphi_{r,R} & \varphi_{r,Y} & 0 \\ \varphi_{y,R} & \varphi_{y,Y} & 0 \\ 0 & 0 & \varphi_r / R \end{pmatrix} = \begin{pmatrix} u_{r,R} & u_{r,Y} & 0 \\ u_{y,R} & u_{y,Y} & 0 \\ 0 & 0 & u_r / R \end{pmatrix} + \begin{pmatrix} 1 & 0 & 0 \\ 0 & 1 & 0 \\ 0 & 0 & 1 \end{pmatrix}, \tag{22}$$

where the coordinate system (r, y, θ) is defined as: r is the distance from the symmetry axis, y is the symmetry axis, and θ is the angle around the symmetry axis.

Consider now a finite element subdivision of the region Ω_0 into elements Ω_{0e}, $e = 1, \ldots, NEL$ where each element has the interpolation for the updated state $\boldsymbol{\varphi}(\mathbf{X})$ defined as

$$\boldsymbol{\varphi} = \sum_{I=1}^{NODE} N^I(\mathbf{X}) \boldsymbol{\varphi}_e^I \Rightarrow \delta\mathbf{l} = \sum_{I=1}^{NODE} \delta\boldsymbol{\varphi}_e^I \otimes \mathbf{g}^I, \tag{23}$$

where $\mathbf{g}^I = \mathbf{G}^I \cdot \mathbf{F}^{-1}$ and $\mathbf{G}^I = \nabla_{\mathbf{X}} \mathbf{N}^I$ are the spatial and material gradients of shape functions, respectively, and *NODE* is the number of nodes. Upon inserting the discretisation into the weak form of the momentum balance (20), the discrete formulation is obtained as

$$\mathop{\mathbf{A}}_{e=1}^{NEL} \left(\mathbf{b}_e - \mathbf{f}_e^{ext} \right) = 0, \tag{24}$$

where the assembly operator **A** defines to the element global node topology. In (24), the finite element vectors are defined as

$$\mathbf{b}_e = \mathop{\mathbf{A}}_{I=1}^{NODE} \int_{\Omega_{0e}} (\boldsymbol{\tau} - J\, p\mathbf{1}) \cdot \mathbf{g}^I R\, d\Omega \text{ and } \mathbf{f}_e^{ext} = \mathop{\mathbf{A}}_{I=1}^{NODE} \int_{\partial\Omega_{0e}} -p^{ext} \mathbf{N}^I \cdot J\mathbf{F}^{-t} \cdot \mathbf{N} R\, dL, \tag{25}$$

where ***A*** defines the internal topology between element variables and the tensorial quantities, i.e.

$$\delta\mathbf{l} : \bar{\boldsymbol{\tau}} = \sum_{I=1}^{NODE} \delta\boldsymbol{\varphi}_e^I \cdot \bar{\boldsymbol{\tau}} \cdot \mathbf{g}^I = \delta\hat{\boldsymbol{\varphi}}_e^t \mathop{\mathbf{A}}_{I=1}^{NODE} \bar{\boldsymbol{\tau}} \cdot \mathbf{g}^I. \tag{26}$$

The incrementally nonlinear FE equations (26) are solved using Newton-Raphson's method, whereby it is required that each Newton iterative ξ_e at the element level satisfies the relation

$$\mathop{\mathbf{A}}_{e=1}^{NEL} \delta\hat{\boldsymbol{\varphi}}_e^t \left(\left(\mathbf{b}_e - \mathbf{f}_e^{ext} \right) + \mathop{\mathbf{A}}_{e=1}^{NEL} \mathbf{K}_e \boldsymbol{\xi}_e \right) = 0, \tag{27}$$

where $\mathbf{K}_e$ is the element stiffness matrix defined as $\mathbf{K}_e = \mathbf{K}_e^{\text{int}} - \mathbf{K}_e^{ext}$. The internal and external stiffness matrices, $\mathbf{K}_e^{\text{int}}$ and $\mathbf{K}_e^{ext}$, are derived using equation (21) as

$$\mathbf{K}_e^{\text{int}} = \underset{I=1}{\overset{NODE}{A}} \underset{J=1}{\overset{NODE}{A}} \int_{\Omega_0} \mathbf{g}^I \cdot \Big(\mathbf{E}_2 + \mathbf{1} \bar{\otimes} \bar{\boldsymbol{\tau}} - J\, p \left(\mathbf{1} \otimes \mathbf{1} - 2\mathbf{I}^{sym} \right) + K^s \left(J / J - \left(1 - n_0^s \right) \right) \mathbf{1} \otimes \mathbf{1} \Big) \cdot \mathbf{g}^I \; Rd\Omega,$$

$$\mathbf{K}_e^{ext} = \underset{I=1}{\overset{NODE}{A}} \underset{J=1}{\overset{NODE}{A}} \int_{\partial\Omega_0} p^{ext} N^I \left(J\mathbf{F}^{-t} \cdot \mathbf{N} \otimes \mathbf{1} - \left(\mathbf{F}^{-t} \underline{\otimes} \left(\mathbf{F}^{-t} \cdot \mathbf{N} \right) \right) \cdot \mathbf{F}^t \right) \cdot \mathbf{g}^I \; RdL. \tag{28}$$

4. BOUNDARY VALUE PROBLEM

In the following example the developed methodology is used for process modelling of an axisymmetric pressure vessel. The preform consists of a combination of braided and winded layers. The implemented constitutive model is based on a series of tests performed on the commingled GF/PP Twintex R PP 75 AF material, [2], and are summarised in Table 1. The material data are obtained for the following processing conditions: temperature 190°C, consolidated for 20 minutes and quenched for 120 seconds down to a temperature of 60°C. Intra-bundle permeability was computed using the model for unidirectional reinforcement by Gebart [5].

Table 1. The material parameters for the Twintex R PP 75 AF material

Param	E [GPa]	k^s	m^s	k^b	m^b	ϕ_0	ζ [μm]	μ [Pa/s]	G [MPa]
Value	75	0.0033	15.5	0.0093	15.5	0.685	200	410	5.8

In Table 1, E refers to the Young's modulus of the fibres and k^s and k^b are nondimensional front factors for the fibre bundles and the fibre bundle network response, respectively. m^s and m^b are nondimensional exponents used in the fibre packing equation [3]. ϕ_0 is the fibre volume fraction in the bundles of the reference configuration (undeformed). Finally, ζ is the material characteristic length of infiltration, μ is the resin viscosity and G is the shear modulus of the fibre bundle network.

In the present example, the finite-element analysis of undrained consolidation of the axisymmetric composite pressure vessel, as shown in Figure 3a, is considered. Consolidation pressure is applied on the inner surface of the pressure vessel. Two different pressure levels are considered: 1 bar and 8 bars, respectively. In order to emulate the loading on the vessel, the pressure is applied during a time period of 1 second and kept constant at the nominal level afterwards (1800 seconds for the 1 bar load case and 120 seconds for the 8 bars load case). The outer boundary, in accordance with the real case, is constrained in all degrees of freedom. The finite element formulation is accomplished using a mesh of 265 CST-elements.

4. RESULTS

The results from the simulations are presented in Figure 3 and Figure 4. Figure 3 shows the evolution of the degree of infiltration versus time at the two pressure levels. Results are presented at five different locations, defined in Figure 3a. Figures 3b and c show the evolution of infiltration at 1 and 8 bars, respectively.

It is observed that of infiltration at 1 bar is very slow. For instance, the maximum degree of infiltration at $t = 200$ [sec] is less than 0.5. An acceptable level of infiltration, say $\xi \geq 0.7$, is achieved after about 30 minutes (results not shown in the figure). However, the pressure vessel processed at 8 bar shows significantly higher rates of

infiltration. The region of the neck where the pressure load acts along the y-axis, i.e. element 14, is fully infiltrated after two minutes. Moreover, at $t = 120$ [sec] almost the entire vessel is infiltrated to $\xi \approx 0.6$, one exception being the inside of the neck, element 22, where the degree of infiltration is $\xi \approx 0.4$. Finally, considering the results in element 134 it is concluded that its rate of infiltration is very high during the first 20 seconds, where after it slows down considerably – never reaching full consolidation. This observation applies for both load cases, however this phenomenon is most pronounced for the second load case.

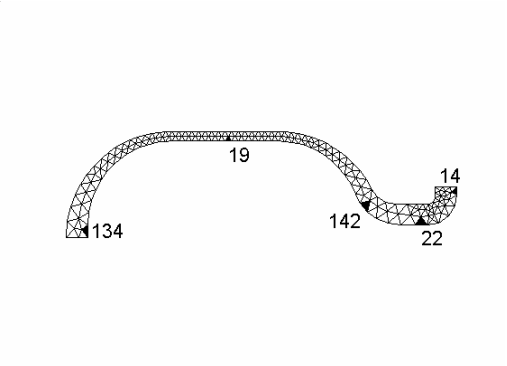

(a) The five elements used for the subsequent graphs

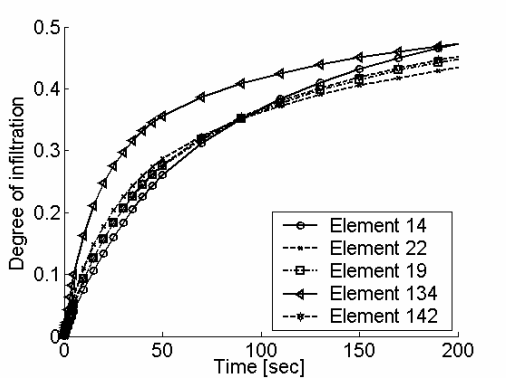

(b) Evolution of degree of infiltration at 1 bar.

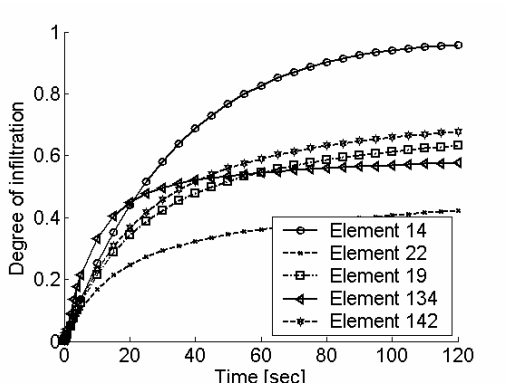

(c) Evolution of degree of infiltration at 8 bar.

Figure 3. The degree of infiltration vs. time for the five selected elements, as defined in (a).

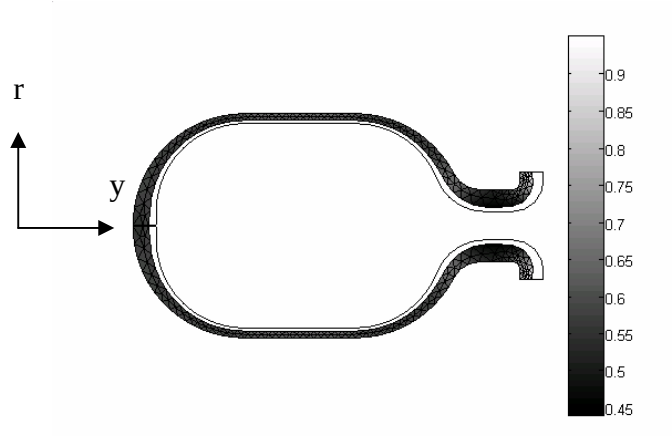

Figure 4. Degree of infiltration and deformation pattern at the final time step.

Figure 4 shows the deformed vs. undeformed geometry as well as the infiltration at the final load-step, $t = 120$ [sec], for the 8 bar case. In consistence with the results shown in the Figure 3c the degree of infiltration, at the same time step, is both highest and lowest at the neck of the vessel.

5. DISCUSSION AND CONCLUDING REMARKS

In this paper a finite element code for modelling of pressure driven axisymmetric consolidation of commingled PP/GF yarns is presented. For this purpose a two-phase continuum model in a FE-framework is employed and computational results from a numerical example (pressure vessel) are presented for two levels of consolidation pressure.

The first analysis was aimed to simulate a composite process performed at a pressure of 1 bar, e.g. a case of vacuum assisted consolidation. The second analysis was performed at 8 bar, e.g. simulation of an autoclave process. The results clearly show that the pressure obtained using vacuum only is inadequate for successful pressure vessel manufacturing.

The computational results, in general, show a highly uneven infiltration rate in the region of the neck, see Figure 4. It is concluded that the small radius and thick wall at the centre of the neck intensify the effects of axial symmetry. Evidently, high tangential stresses carried by fibres in the neck unload the fluid, and therefore prevent infiltration. Moreover, consolidation in the opening (element 14), where the pressure acts along the y-axis, c.f. Figure 4, is marginally affected by the tangential stresses and therefore infiltrates more rapidly. Finally, in the middle of the pressure vessel (element 19), the radius is larger and the thickness smaller. Consequently the effects of axial symmetry in that region are less pronounced and a more uniform and rapid consolidation is obtained. The bottom of the vessel exhibits a somewhat unexpected behaviour, see element 134. During the first twenty seconds of consolidation this region shows the highest rate of infiltration. Subsequently, the process basically comes to a standstill and that element exhibits the slowest infiltration. The latter is due to high membrane stresses caused by the ongoing infiltration, void exclusion and volume reduction. These stresses unload the fluid and consequently inhibit further infiltration in the bottom region.

The simulation shows that the bottle may be difficult to manufacture for the chosen preform configuration. In general, the consolidation of the whole vessel, except at the opening, is prevented by the loading mode where the pressure is applied on the interior.

This introduces extensive tangential stresses, which unload the fluid pressure and slow the infiltration down.

To succeed in manufacturing of this type of pressure vessel we suggest using an oversized preform that allows extension in the fibre direction. As a consequence the fluid pressure will not unload and the rate of infiltration will remain unaffected throughout the process. A trade-off with this approach is, however, that the fibres and fibre-bundles may become undulated, lowering the mechanical properties of the pressure vessel.

In conclusion, the present study demonstrates the feasibility of a multidisciplinary modelling approach, where material science is combined with multiphase solid mechanics. Starting from theoretical foundations, mechanistic constitutive models have been developed. These models have then been implemented within the framework of large strain finite element theory for axisymmetric problems. Finally, the material parameters together with the computational models have been used to predict the state of deformation and consolidation of a pressure vessel during manufacturing.

REFERENCES

[1] Gibson, A.G., Månson, J.A.E., "Impregnation technology for thermoplastic matrix composites", *Composites Manufacturing*, 1992, vol. 3, pp. 223-233.

[2] Wysocki, M., "Continuum Modelling of Composites Consolidation", *PhD Thesis*, Chalmers University of Technology, 2006.

[3] Larsson, R., Wysocki, M., Toll, S., "Process-modelling of composites using two-phase porous media theory", *European Journal of Mechanics A/Solids*, 2004, vol. 23, pp. 15-36.

[4] Larsson, J., Larsson, R., "Non-linear analysis of nearly saturated porous media: Theoretical and numerical formulation", *Computer Methods in Applied Mechanics and Engineering*, 2002, 191, Vol. 36, pp. 3885-3907.

[5] Gebart, B.R., "Permeability of unidirectional reinforcement for RTM", *Journal of Composite Materials*, 1992, Vol. 26, pp. 1100-1133.